The Astrophysical Journal, 897:67 (11pp), 2020 July 1 https://doi.org/10.3847/1538-4357/ab919b

Accurate Treatment of Comptonization in X-Ray Illuminated Accretion Disks

Javier A. García[1,2], Ekaterina Sokolova-Lapa[2,3], Thomas Dauser[2], Jerzy Madej[4], Agata Różańska[5], Agnieszka Majczyna[6], Fiona A. Harrison[1], and Jörn Wilms[2]
[1] Cahill Center for Astronomy and Astrophysics, California Institute of Technology, Pasadena, CA 91125, USA; javier@caltech.edu
[2] Dr. Karl Remeis-Observatory and Erlangen Centre for Astroparticle Physics, Sternwartstr. 7, D-96049 Bamberg, Germany
[3] Sternberg Astronomical Institute, M. V. Lomonosov Moscow State University, Universitetskij pr., 13, Moscow 119992, Russia
[4] Astronomical Observatory, University of Warsaw, Al. Ujazdowskie 4, 00-478 Warszawa, Poland
[5] Nicolaus Copernicus Astronomical Center, Polish Academy of Sciences, Bartycka 18, 00-716 Warszawa, Poland
[6] National Centre for Nuclear Research, ul. Andrzeja Sołtana 7, 05-400 Otwock, Poland
Received 2020 March 14; revised 2020 May 7; accepted 2020 May 8; published 2020 July 2

Abstract

A large fraction of accreting black hole and neutron star systems present clear evidence of the reprocessing of X-rays in the atmosphere of an optically thick accretion disk. The main hallmarks of X-ray reflection include fluorescent K-shell emission lines from iron (∼6.4–6.9 keV), the absorption iron K-edge (∼7–9 keV), and a broad featureless component known as the Compton hump (∼20–40 keV). This Compton hump is produced as the result of the scattering of high-energy photons ($E \gtrsim 10$ keV) of the relatively colder electrons ($T_e \sim 10^5$–10^7 K) in the accretion disk, in combination with photoelectric absorption from iron. The treatment of this process in most current models of ionized X-ray reflection has been done using an approximated Gaussian redistribution kernel. This approach works sufficiently well up to ∼100 keV, but it becomes largely inaccurate at higher energies and at relativistic temperatures ($T_e \sim 10^9$ K). We present new calculations of X-ray reflection using a modified version of our code `xillver`, including an accurate solution for Compton scattering of the reflected unpolarized photons in the disk atmosphere. This solution takes into account quantum electrodynamic and relativistic effects allowing the correct treatment of high photon energies and electron temperatures. We show new reflection spectra computed with this model, and discuss the improvements achieved in reproducing the correct shape of the Compton hump, the discrepancies with previous calculations, and the expected impact of these new models in the interpretation of observational data.

Unified Astronomy Thesaurus concepts: Accretion (14); Stellar accretion disks (1579); Atomic spectroscopy (2099); Radiative transfer simulations (1967); Astronomical simulations (1857); Black hole physics (159)

1. Introduction

Accretion onto compact objects such as black holes or neutron stars is one of the most efficient mechanisms to convert gravitational energy into radiation. This radiation is mostly comprised of very energetic photons, making X-ray spectroscopy a flexible technique to study these systems and their interaction with the surrounding material. In the case of black holes, the X-ray continuum is typically dominated by non-thermal emission in the form of a power-law that extends to high energies, which is thought to be produced either in a centrally located and hot ($T_e \sim 10^9$ K) plasma, the origin of which is still a matter of debate (e.g., Shakura & Sunyaev 1973; Matt et al. 1992; Haardt 1993; Markoff et al. 2005). Thermal emission from the accretion disk can peak from the ultraviolet band to the soft X-rays, depending on the mass of the black hole.

A fraction of the non-thermal emission illuminates the accretion disk, producing a rich reflection spectrum of fluorescent lines and other spectral features. This reflection component can appear ionized, with the most prominent spectral lines being due to Fe K emission at 6.4–6.9 keV (e.g., Ross & Fabian 2005; García & Kallman 2010). These features can also be severely distorted in the strong-gravity regime by the Doppler effect, light bending, and gravitational redshift (e.g., Fabian et al. 1989; Laor 1991). Relativistically broadened Fe K lines have been observed in the spectra of the majority of well-studied black hole binaries, as well as in a large fraction of active galactic nuclei (e.g., Brenneman 2013; Reynolds 2019).

At energies well above the Fe K-threshold (∼7–9 keV), the photoelectric cross section of the metals decreases rapidly and electron scattering becomes the dominant source of opacity. Thus, high-energy photons will suffer several scatterings with the electrons in the upper layers of the accretion disk. Here, we only consider high-energy photons with energies less than 1.022 MeV (twice the electron rest mass), because we do not treat electron–positron pair production. These photons lose energy after every scattering, roughly a Compton wavelength per event ($\lambda_C = h/m_e c \approx 0.024$ Å, where h is the Planck's constant, m_e is the electron rest mass, and c is the speed of light). Since electrons are not at rest (particularly if the gas temperature T_e is high), photons will lose an additional fractional energy per scattering ($\Delta E/E \sim 3kT_e/m_e c^2$). The reduction of the number of photons at high energies due to electron scattering, and at lower energies due to the photoelectric opacity of iron, leads to a broad and featureless spectral feature centered around 20–30 keV, typically referred to as the Compton hump (Guilbert & Rees 1988; Lightman & White 1988). This distinct feature is considered one of the hallmarks of X-ray reflection in optically thick media.

A detailed calculation of the redistribution of high-energy photons due to Compton scattering is crucial to correctly predict the detailed spectral shape of X-ray reprocessed in accretion disks. One of the most accurate methodologies to solve the Comptonization problem is via Monte Carlo calculations, where individual photons are "followed" as they interact with the electrons in the gas (e.g., George & Fabian 1991; Matt et al. 1991, 1993). The

Monte Carlo method has the advantage that it treats the radiative transfer problem exactly (within the numerical precision), given that no other source of opacity is considered. However, the drawback is that it is computationally expensive, and becomes prohibitive when the complexity of the microphysics is increased (e.g., when atomic lines are also considered). Thus, in cases where the coupling between the radiation and the medium is described with enough physics, the price to pay is the implementation of more approximated methods to solve the radiation transfer.

The complete problem of reflected (reprocessed) X-rays in optically thick media such as accretion disks has been a subject of study for nearly four decades now. Among the most popular models are `reflionx` (Ross & Fabian 2005) and `xillver` (García & Kallman 2010; García et al. 2011, 2013). Until now, these models have treated the redistribution of photons due to Compton scattering in a rather approximated fashion, using a simple redistribution function based on a Gaussian profile (e.g., Ross & Fabian 1993; Nayakshin et al. 2000; García & Kallman 2010). This approximation allows for a fast calculation of the photon redistribution at each depth in the atmosphere, which is particularly challenging when the required energy resolution of the model is high. However, the Gaussian approximation becomes increasingly inaccurate at energies close to or above the electron rest-mass energy ($m_e c^2 = 511$ keV), or at very high temperatures where the thermal motion of electrons becomes relativistic, which causes a suppression of the scattering cross section below the Klein–Nishina prediction (Madej et al. 2017).

The redistribution function accurate for photon energies approaching electron rest mass, was given by Guilbert (1981) and used by Madej & Różańska (2000), and Madej & Różańska (2004) in the case of irradiated stellar atmospheres in hydrostatic and radiative equilibrium. Furthermore, this procedure was adopted for the stratified accretion disk atmosphere, but with a limited number of atomic opacities (Różańska & Madej 2008; Różańska et al. 2011).

In this paper we present new calculations of the redistribution function due to electron scattering as a function of photon energy and electron temperature, implementing an accurate solution that takes into account quantum electrodynamic and relativistic effects, allowing the correct treatment of high photon energies and electron temperatures. A detailed comparison with the standard Gaussian approximation is also presented. Moreover, we implement this new solution into our reflection model `xillver` and discuss the discrepancies with previous calculations, and the expected impact of these new models in the interpretation of observational data.

The remainder of the paper is organized as follows. In Section 2 we outline the basic approach for the radiative transfer calculations, and describe in detail the expressions used for the redistribution of photons due to Compton scattering. In Section 3 we show the main results, including a comparison of the Gaussian and exact solutions in the convolution of a single radiation field, several iterations, and reflection calculations done at different levels of complexity. A discussion of these calculations and our main conclusions are presented in Section 4.

2. Numerical Calculations

2.1. Radiative Transfer

There exists an extensive literature on the problem of radiation transfer in opaque media. The reader is referred to review such works, in particular Chandrasekhar (1960), Mihalas (1978), and Hubeny & Mihalas (2014), which are considered the seminal works in the field. Here, we only discuss the general equations in order to describe the problem at hand.

In the one-dimensional case applicable to plane-parallel atmospheres, the standard form of the radiative transfer equation in steady state can be written as

$$\mu \frac{\partial I(E, \mu)}{\partial \tau(E)} = I(E, \mu) - S(E), \tag{1}$$

with $\mu = \cos\theta$, where θ is the angle between the direction of propagation of the intensity $I(E, \mu)$ and the spatial coordinate. In Equation (1) we have omitted the explicit dependence on the optical depth τ, which is the energy-dependent opacity $\chi(E)$ of the material along the line of sight:

$$\tau(E) = \int -\chi(E) dz. \tag{2}$$

In general, both absorption and scattering processes contribute to the total opacity, $\chi(E) = n_e(\sigma_a + \sigma_s)$, where n_e is the electron number density, and σ_a and σ_s are the absorption and scattering cross sections, respectively.

The source function $S(E)$ is defined as the ratio of the total emissivity, $\eta(E) = n_e[\sigma_a B(E, T) + \sigma_s J_c(E)]$, to the total opacity:

$$S(E) = \frac{\sigma_a B(E, T) + \sigma_s J_c(E)}{\sigma_a + \sigma_s}. \tag{3}$$

Here, the first term represents the gas emissivity assuming local thermal equilibrium, where $B(E, T)$ is Planck's function at the local temperature. The second term is the emissivity due to electron scattering,[7] which is proportional to the Comptonized mean intensity of the radiation field, resulting from the convolution

$$J_c(E) = \frac{1}{\sigma_s} \int dE' J(E') R(E', E), \tag{4}$$

where $J(E) = \frac{1}{2}\int_{-1}^{+1} d\mu I(E, \mu)$ is the first moment of the radiation field, and $R(E', E)$ is the *redistribution function*, which represents the probability that a photon will be scattered from an energy E' to an energy E. For the purposes of this paper, we consider this redistribution to be isotropic, i.e., independent of the direction of the incoming and outgoing photon. The presence of scattering terms in the radiative transfer equation is one of the main difficulties in the solution of real physical problems, as it decouples the radiation field from the local properties of the material, allowing photons to be transported over large distances.

2.2. The Redistribution Function

After an inelastic scattering event with an electron, an X-ray photon can gain or lose energy. The energy exchange depends on the initial photon energy, and on the electron temperature. The probability for a photon with energy E_i to have an energy E_f after the scattering is given by the *redistribution function*, $R(E_i, E_f)$. Integration of this function over the final photon

[7] In general, other scattering events could be considered, such as Rayleigh scattering due to molecules, but in the context of X-ray-illuminated accretion disks, these are negligible.

energies results in the energy-dependent Compton scattering cross section:

$$\sigma_{\rm CS}(E_i) = \sigma_{\rm T} \int R(E_i, E_f) dE_f, \quad (5)$$

where $\sigma_{\rm T} \approx 6.65 \times 10^{-25}\,{\rm cm}^2$ is the classical Thomson scattering cross section (Thomson 1906).

There are a number of different redistribution functions used in the literature to describe the probability of a photon with initial energy E_i being scattered off an electron with final energy E_f. The most complete and detailed review of the different approximations for Compton scattering redistribution functions and their limitations was given by Madej et al. (2017). Here, we will focus on two of the most relevant forms: the exact quantum mechanical formula for relativistic electrons; and the Gaussian approximation for thermal Compton scattering, as first implemented in the problem of X-ray reflection by Ross et al. (1978). Next, these two solutions are described in detail.

2.2.1. The Exact Redistribution Function

The first expression for the exact formula of the redistribution function was obtained by Jones (1968), and later corrected by Aharonian & Atoyan (1981). Since then, a number of works have discussed different ways to simplify the given equation and to perform an accurate integration (e.g., Kershaw et al. 1986; Nagirner & Poutanen 1993, 1994). Here, we adopt the second exact form given by Nagirner & Poutanen (1993) (hereafter NP93),

$$R_{\rm E}(x, x_1, \mu, \gamma) = \frac{2}{Q} + \frac{u}{v}\left(1 - \frac{2}{q}\right) + u\frac{(u^2 - Q^2)(u^2 + 5v)}{2q^2v^3} + u\frac{Q^2}{q^2v^2}, \quad (6)$$

where x, x_1 are the dimensional photon energies before and after the scattering, μ is the cosine of the scattering angle, γ is the electron Lorenz factor, $q = xx_1(1 - \mu)$, and $Q^2 = (x - x_1)^2 + 2q$. The functions u and v are defined through

$$a_-^2 = (\gamma - x)^2 + \frac{1 + \mu}{1 - \mu} \quad (7)$$

and

$$a_+^2 = (\gamma + x_1)^2 + \frac{1 + \mu}{1 - \mu}, \quad (8)$$

as

$$u = a_+ - a_- = \frac{(x + x_1)(2\gamma + x_1 - x)}{a_- + a_+} \quad (9)$$

and

$$v = a_- a_+, \quad (10)$$

in order to avoid the accuracy loss due to numerical cancellation (see the detailed overview given by Madej et al. 2017, Section 3.2). The resulting redistribution function for Compton scattering is obtained by integrating Equation (6) with the relativistic Maxwellian distribution

$$R_{\rm E}(x, x_1, \mu) = \frac{3}{32\mu\Theta K_2(1/\Theta)} \int_{\gamma_*}^{\infty} R_{\rm E}(x, x_1, \mu, \gamma) \exp(-\gamma/\Theta) d\gamma, \quad (11)$$

where K_2 is a modified Bessel function of the second kind (the Macdonald's function), and the lower limit of the integral is $\gamma_* = (x - x_1 + Q\sqrt{1 + 2/q})/2$.[8] We refer to the redistribution function given by Equation (11) as *exact* in the following, in the sense that it includes all the necessary physical effects, though it is not free of the computational errors inserted by numerical calculations. We also note that we neglect pair production for energies greater than 1.022 MeV.

2.2.2. The Gaussian Redistribution Function

In the case of relatively low photon energies ($E \ll m_e c^2$), and for electron temperatures much lower than the photon field ($kT_e \ll E$), a simple approximation can be implemented, in which scattered photons are assumed to be distributed according to a Gaussian profile. This idea was first introduced by Dirac (1925) and later by Münch (1948) in order to take into consideration the velocity of thermal agitation of electrons in stellar atmospheres.

As described in Ross & Fabian (1993), the probability of a photon with initial energy E_i being scattered to a final energy E_f can be written as

$$P(E_i, E_f) = \frac{1}{\sqrt{2\pi}\Sigma} \exp\left[-\frac{-(E_f - E_c)^2}{2\Sigma^2}\right], \quad (12)$$

with centroid energy E_c given by

$$E_c = E_i\left(1 + \frac{4kT}{m_{\rm e}c^2} - \frac{E_i}{m_{\rm e}c^2}\right), \quad (13)$$

and the standard deviation

$$\Sigma = \Sigma(E_i) = E_i\left[\frac{2kT}{m_{\rm e}c^2} + \frac{2}{5}\left(\frac{E_i}{m_{\rm e}c^2}\right)^2\right]^{1/2}. \quad (14)$$

This Gaussian approximation was first used in the context of photoionization models by Ross (1978) and Ross et al. (1978), who later implemented into the reflection model `reflion` (Ross & Fabian 1993), and its subsequent incarnations `reflionx` (Ross & Fabian 2005), `refbhb` (Ross & Fabian 2007), and several other calculations based on the same code (Ballantyne et al. 2001, 2002, 2004, 2005, 2012; Ballantyne 2004). Likewise, the same approximation was used in calculations using the XSTAR photoionization code (Kallman & Bautista 2001) to solve the X-ray reflection problem in hydrostatic atmospheres (Nayakshin et al. 2000; Nayakshin & Kallman 2001); and more recently in the constant density reflection calculations using the `xillver` code (García & Kallman 2010; García et al. 2011, 2013, 2014, 2016).

In all the works mentioned above, the normalization of the probability function has been chosen such that the integral over the redistribution function gives the Klein–Nishina cross

[8] We note that there is a misprint in the definition of γ_* in Madej et al. (2017), Equation (4). See the erratum Madej et al. (2019).

section $\sigma_{\rm KN}(E_i)$

$$R_{\rm G}(E_i, E_f) = \frac{P(E_i, E_f)\sigma_{\rm KN}(E_i)}{\int P(E_i, E_f)dE_f}, \quad (15)$$

which can be explicitly written as

$$\sigma_{\rm KN}(x) = \sigma_{\rm T}\frac{3}{4}\left\{\frac{1+x}{x^3}\left[\frac{2x(1+x)}{1+2x} - \ln(1+2x)\right] + \frac{1}{2x}\ln(1+2x) - \frac{1+3x}{(1+2x)^2}\right\}, \quad (16)$$

where $x = E/m_{\rm e}c^2$ (Klein & Nishina 1929). As we show next, this normalization needs to be adjusted in order to compare with the exact solution.

2.3. Normalization of the Redistribution Functions

In order to compare the Gaussian approximation with the exact solution of the redistribution function, one needs to make sure that they are both normalized in such a way that the integrals $\int R_{\rm G}(E_i, E_f)dE_f$ and $\int R_{\rm E}(E_i, E_f)dE_f$ yield the same total scattering cross section. At low enough electron temperatures ($T \lessapprox 1 \times 10^7$ K), these integrals are equal to the Klein–Nishina cross section $\sigma_{\rm KN}(E_i)$.

However, at higher temperatures the thermal motion of relativistic electrons in hot plasma becomes important and needs to be taken into account. The Compton scattering cross section convolved with a relativistic Maxwellian distribution of electrons was written by Poutanen et al. (1996) as

$$\sigma_{\rm CS}(x) = \frac{3\sigma_{\rm T}}{16x^2\Theta K_2(1/\Theta)}\int_1^\infty e^{-\gamma/\Theta}\left\{\left(x\gamma + \frac{9}{2} + \frac{2\gamma}{x}\right)\times \ln\left[\frac{1+2x(\gamma+z)}{1+2x(\gamma-z)}\right] - 2xz + z\left(x - \frac{2}{x}\right)\ln(1+4x\gamma+4x^2) + \frac{4x^2z(\gamma+x)}{1+4x\gamma+4x^2} - 2\int_{x(\gamma-z)}^{x(\gamma+z)}\ln(1+2\xi)\frac{d\xi}{\xi}\right\}d\gamma, \quad (17)$$

where $\Theta = kT/m_ec^2$ and $z = \sqrt{\gamma^2-1}$.

We calculated the total cross section in Equation (17) using a 20-point Gauss–Legendre quadrature for the internal integral over ξ, and a 200-point Gauss–Laguerre quadrature for the integral over γ. Figure 1 shows a comparison of the total cross section averaged over the relativistic Maxwellian distribution for different electron temperatures, the classical Thomson, and the Klein–Nishina cross sections.

In order to have a meaningful comparison, we normalize the two redistribution functions (exact and Gaussian) to the energy-dependent cross section $\sigma_{\rm CS}$ in the usual way:

$$R_{\{\rm E,G\}}(E_i, E_f) = \frac{\sigma_{\rm CS}(E_i)}{\sigma_{\rm T}}\frac{R_{\{\rm E,G\}}(E_i, E_f)}{\int R_{\{\rm E,G\}}(E_i, E_f)dE_f}. \quad (18)$$

We note that the integration over final energies of the exact redistribution function (from NP93), multiplied by the Thomson scattering cross section, should itself give the cross section $\sigma_{\rm CS}(E)$. But accounting for the finiteness of the grids used later for radiative transfer calculation, and thus the errors in numerical integration over angles and γ, the normalization is still required.

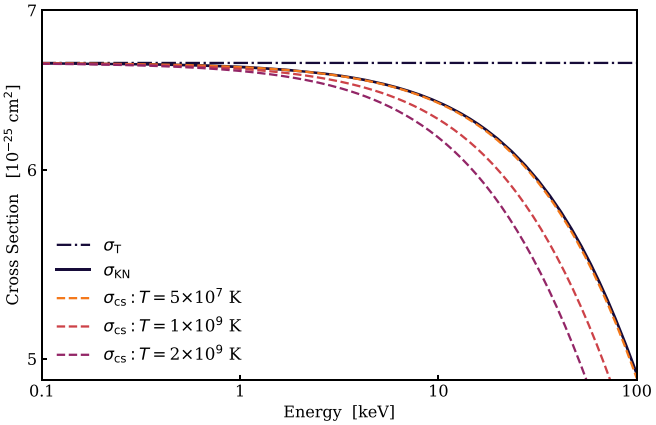

Figure 1. Comparison of the total quantum electrodynamic Klein–Nishina cross section for Compton scattering of photons off stationary electrons (Klein & Nishina 1929), and the Klein–Nishina cross section convolved with a relativistic Maxwellian (Poutanen et al. 1996). As expected, the largest deviations occur at high electron temperatures.

Figure 2 shows a comparison of the redistribution functions computed with the Gaussian approximation and the exact solution using the above normalization. We used up to a 3000-point Gauss–Legendre quadrature to integrate the redistribution function Equation (11) over the scattering angle. The integral over γ is computed using a 32-point Gauss–Laguerre quadrature after setting the new variable $u = (\gamma - \gamma_*)/\Theta$, as discussed in Madej et al. (2017). The modified Bessel function has to be treated with care, thus at the limiting cases we used asymptotic expansions, given by Abramowitz et al. (1988). We show comparisons for different initial photon energies and electron temperatures. From this comparison it is evident that the Gaussian approximation works much better at low photon energies and electron temperatures.

For an initial photon of 1 keV, the exact solution is symmetric, thus the Gaussian approximation agrees fairly well, except at very high temperatures ($T \gtrsim 10^8$ K) where the peaks of the distributions are shifted. At higher energies, as the photon approaches m_ec^2, the exact solution becomes double-peaked and more asymmetric, making the differences with the Gaussian approximation more noticeable. When the energy of the photons is much larger than the kinetic energy of the electrons, the solution approaches the case of a single scattering out of electrons at rest. In this limit, the shape of the redistribution function is symmetric and double-peaked, as shown by Lightman et al. (1981). The solution peaks at the initial photon energy, and at the energy of maximum shift, given by twice the Compton wavelength λ_c. In this regime, the Gaussian solution becomes extremely broad, failing to accurately represent the correct redistribution function due to Compton scattering. Nevertheless, up to ∼100 keV, the agreement between the two solutions is acceptable.

3. Results

3.1. Convolution of an Input Spectrum with the Redistribution Functions

We have conducted calculations to estimate the discrepancies between the Gaussian approximation, and the exact solution of the redistribution function discussed in the previous section might affect the resulting spectrum after several scattering events. This is done by convolving an input spectrum

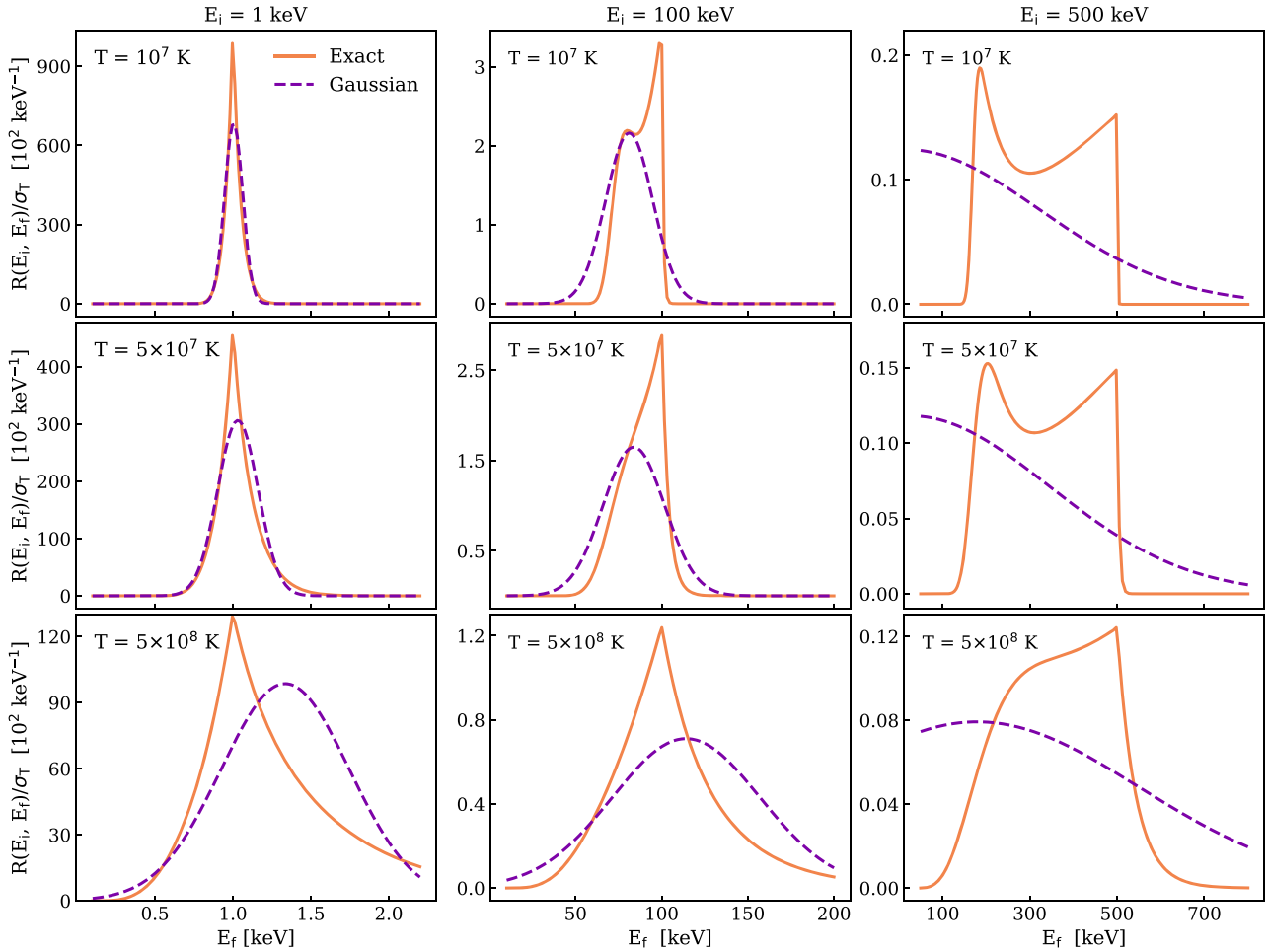

Figure 2. Comparison of the Gaussian approximation for the redistribution of photons after electron scattering events (adopted in several reflection codes such as `reflionx` and `xillver`), and the fully relativistic solution by Nagirner & Poutanen (1993). The two solutions agree well at low energies, but at high energies the discrepancy is dramatic. A similar trend is also observed with respect to the electron temperature.

with each one of two the redistribution functions mentioned above in the following way:

$$J_c^n(E_i) = \frac{1}{\sigma_{CS}(E_i)} \int_{E_{min}}^{E_{max}} dE_f J_c^{n-1}(E_f) R(E_f, E_i), \qquad (19)$$

where n is the number of scattering events. For $n = 1$, $J_c^{n-1}(E)$ represents the input spectral distribution of photons propagating through scattering medium. Notice that in the scattering integral of Equation (19) the inverse redistribution function $R(E_f, E_i)$ needs to be used (rather than $R(E_i, E_f)$). This is because the integrand requires the probability that a photon from any other energy E_f is scattered into the current energy of interest E_i. Importantly, this similar convolution procedure is required during the solution of the transfer equation in reflection codes such as `xillver`. We shall come back to the discussion of these calculations in the following sections.

Figure 3 shows the results for an input power law with a high-energy cutoff in the form $F(E) \propto E^{-(\Gamma-1)}\exp(-E/E_{fold})$, with $E_{fold} = 300$ keV, $\Gamma = 2$ (similar to the canonical input spectra used in the reflection calculations). The convolution is done 300 times to account for multiple scatterings. At a relatively low temperature ($T = 5 \times 10^{6-7}$ K), the result calculated using the Gaussian approximation is very close to the one obtained with fully relativistic redistribution function. However, at higher temperatures ($T = 10^9$ K), the discrepancies are much more dramatic, with strong deviations from the exact solution in the entire energy range.

After many iterations the synthetic spectrum reaches some saturation, approaching a Wien distribution peaking at $E \approx 2.8kT_e$, which is expected for the case of the saturated Comptonization (Sunyaev & Titarchuk 1980; Hua & Titarchuk 1995). Figure 4 shows the gradual changes in the spectra while approaching some equilibrium condition for both redistribution functions discussed above.

3.2. Radiative Transfer Calculations

We now test the effects of the different solutions for the redistribution of photons due to Compton scattering in the final solution of the X-ray spectrum reflected from the surface of an accretion disk. To this end we make use of the routines in our reflection code `xillver`. This model assumes a plane-parallel geometry for a constant density slab of a few Thomson depths (typically $\tau_T \sim 10$). The radiative transfer is solved using the Feautrier method with two boundary conditions for the incident field at the top and bottom of the atmosphere. A detailed description of the numerical methods employed in the `xillver` code can be found in our previous publications (García & Kallman 2010; García et al. 2013, 2014).

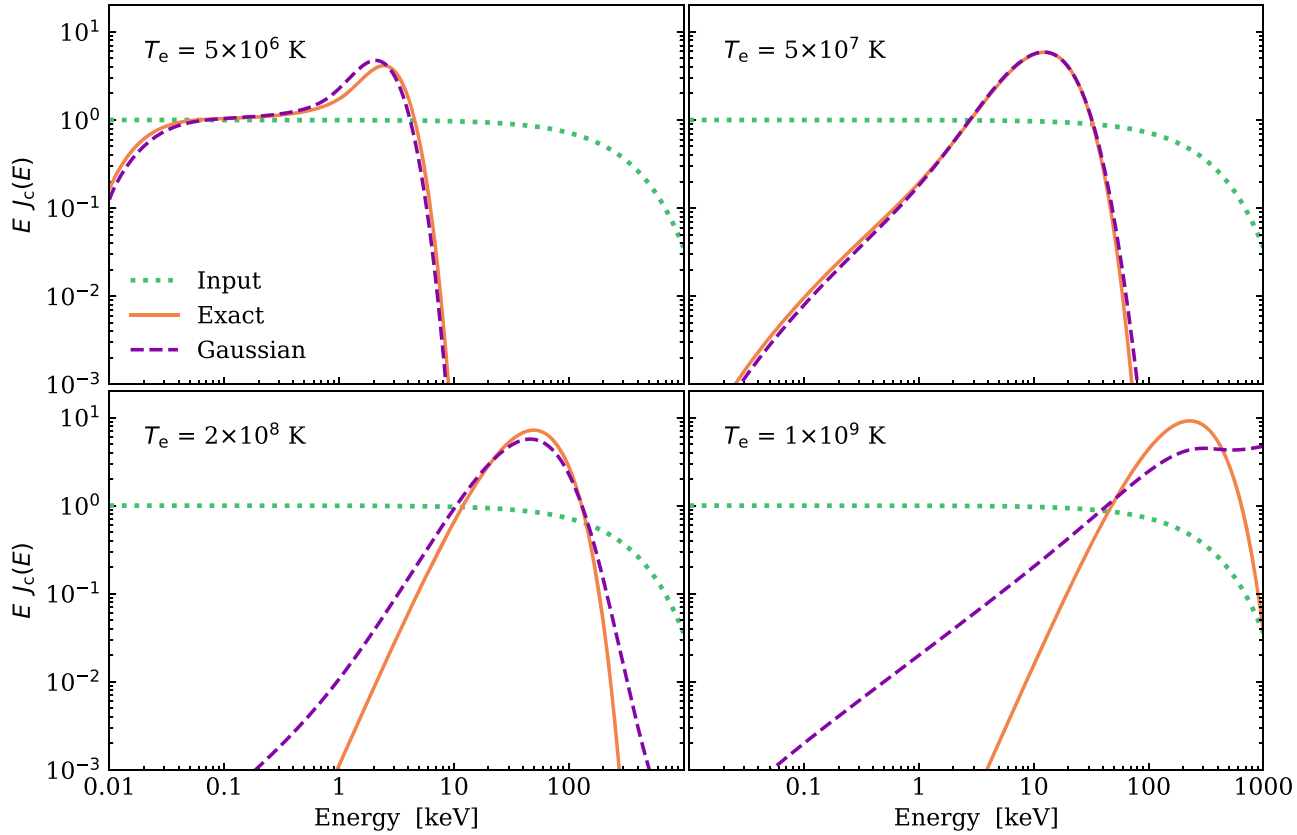

Figure 3. The result of 300 convolutions (Equation (19)) for the input power-law continuum with a high-energy exponential cutoff for the Gaussian approximation (dashed purple line) and the exact solution given by NP93 (solid yellow line). The input spectrum is shown by the dotted green line.

Until now, `xillver` has made use of the Gaussian approximation to account for the redistribution of photons due to Compton scattering. We have now modified these routines to implement the exact solution for the redistribution function by NP93, including relativistic corrections to the total Compton cross section (Poutanen et al. 1996), as described in Section 2.

3.2.1. Pure Scattering Case

In order to test the effects of the new redistribution function, we start with the simple case in which electron scattering is the only source of opacity, and no thermal emission coefficient, i.e., $\sigma_a = 0$. Furthermore, thermal equilibrium is not imposed, such that the gas temperature is kept fixed at a given value. In this configuration, the source function for pure scattering in an isothermal atmosphere is represented by the double integral:

$$S(E) = J_c(E) = \frac{1}{2\sigma_{\rm CS}} \int dE' R(E', E) \int_{-1}^{1} d\mu I(E', \mu). \quad (20)$$

Based on the comparisons discussed above, we expect that the largest differences appear at high temperatures and photon energies. Thus, calculations were carried out assuming an isothermal atmosphere with a constant number density of $10^{15}\,{\rm cm}^{-3}$. The illumination from above was assumed to be a relatively weak power law with $\Gamma = 2$ at 45° incidence, and a much stronger isotropic blackbody radiation field with $kT = 0.35$ keV entering from below at $\tau_{\rm T} = 10$. This particular choice of illumination is somewhat arbitrary, but it serves to test the effects of the Comptonization in the case of a radiation field of a blackbody type. Such a setup can resemble the case of a bright black hole binary system in the soft state, during which the accretion disk becomes luminous and dominates the emission of the X-ray spectrum (e.g., McClintock & Remillard 2006).

Comparisons of the calculations done with the usual Gaussian approximation and with exact the solution with the `xillver` routines are shown in Figure 5, for three different electron temperatures, $kT_e = 2$, 6, and 10 keV. Comptonization in this hot medium produces a significant modification of the original blackbody field, which becomes more severe at higher electron temperatures. For the coldest case, the Gaussian solution approximates well with the exact solution. However, for the other two cases, large discrepancies are obvious for photon energies above $\sim$100 keV, where the Gaussian approximation underestimates the amount of photons that get scattered to lower energies.

3.2.2. Scattering and True Absorption at Fixed Temperature

We have carried out calculations of reflected spectra, now including all astrophysically relevant atomic transitions (assuming solar abundances), for a slab at constant density ($n_e = 10^{15}\,{\rm cm}^{-3}$) and constant temperature ($T \sim 1$ keV), for three different ionization parameter $\xi = 10$, 10^2, 10^3 erg cm s^{-1}. In this case, we follow a more standard setup for the reflection calculation: the slab is illuminated on the top by a power-law spectrum with $\Gamma = 2$ and a high-energy cutoff at 300 keV. Contrary to the pure scattering models presented in the previous section, in this case no illumination from below is considered. This particular setup resembles the case of a black hole binary in the hard state, during

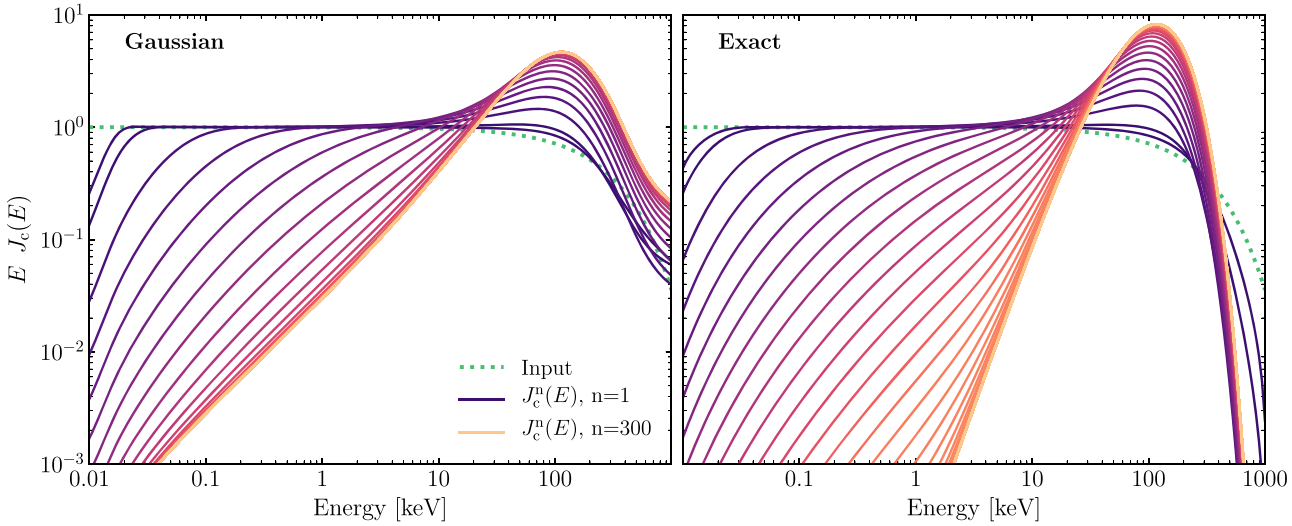

Figure 4. Gradual changes in the resulting spectrum during the performance of the multiple convolutions. $J_c^n(E)$ is shown for every fourth iteration for clarity. The left panel shows the results from the Gaussian approximation, while the right panel shows those from the NP93 exact solution. This figure uses same input spectrum used for Figure 3.

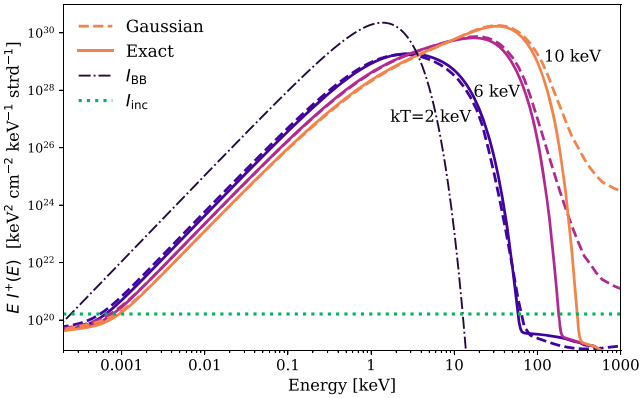

Figure 5. Radiative transfer calculations of an X-ray reflection spectrum from a slab including only Compton scattering (i.e., no atomic contributions, no pair production). The slab is illuminated by a power law at the top, and by strong thermal emission at the bottom. The figure shows three cases for the disk temperature, comparing the exact solution with the previous Gaussian approximation.

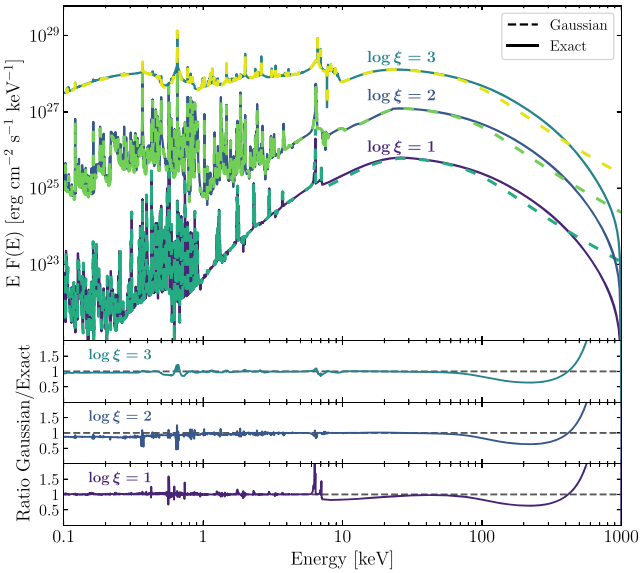

Figure 6. (Top) Angle-averaged reflected spectra calculated with the `xillver` code for a constant density ($n_e = 10^{15}$ cm^{-3}) and isothermal ($T \sim 1$ keV) atmosphere, including both scattering and atomic opacities. The slab is illuminated at the top by a power-law spectrum with $\Gamma = 2$ and a high-energy cutoff at 300 keV. Results for three different ionization parameters ($\xi = 4\pi F_x/n_e = 10, 10^2, 10^3$ erg cm s^{-1}) are presented, using both the Gaussian approximation (dashed curves) and the exact solution (solid curves) by NP93. (Bottom) Ratio of the Gaussian to the exact spectra for each value of the ionization parameter, as indicated.

which the disk emission is faint, while the X-ray spectrum is dominated by a non-thermal power-law like emission (e.g., Remillard & McClintock 2006; McClintock et al. 2013); or the case of reflection in accretion disks around supermassive black holes like the active galactic nuclei of Seyfert galaxies (e.g., Reynolds 2013). This is a common and canonical setup for reflection model calculations (e.g., Ross & Fabian 2005; García & Kallman 2010; García et al. 2013) As before, Compton scattering inside the slab was calculated with the two redistribution functions (Gaussian and exact), keeping the rest of the model unchanged.

Figure 6 shows the comparison of the reflected spectra after 200 Λ-iterations for the radiative transfer solution. As expected, we find that the largest differences are at high energies (above $\sim$100 keV), with the exact solution producing a more curved reflection spectrum compared to the Gaussian approximation. The rest of the reflection spectrum appears mostly unaffected for this particular configuration of parameters. However, a more detailed inspection of the ratio of the Gaussian to the exact solution spectra (Figure 6, bottom panels) shows differences in some of the line profiles. Specifically, the iron K-shell emission lines appear stronger in the Gaussian solution, indicating that the amount of Comptonization in the lines is underestimated. This difference is stronger at low ionization, when the Fe K emission is dominated by the narrower complex of lines at $\sim$6.4 keV (Kα) and $\sim$7.1 keV (Kβ). Some smaller differences are also present at lower energies, in particular for the oxygen Lyα emission at $\sim$0.8 keV.

3.2.3. Complete Reflection Calculations

The ultimate goal is to implement the new and exact solution for the Comptonization into a full reflection calculation. For this, we produced a set of `xillver` models in which we now allow the code to solve the energy and ionization balance equations at each point in the atmosphere. With these models we aim to test the possible secondary effects in the solution due to the change in the energy budget of the radiation field as a consequence of the improved redistribution function. Based on all the previous tests, we expect the largest differences to appear when the irradiated atmosphere reaches the highest temperatures. Thus, we have run models with a larger ionization parameter of $\xi = 3 \times 10^3$ erg cm s^{-1}, while keeping the same gas density of $n_e = 10^{15}$ cm^{-3} (which implies an increase of the net flux incident at the top); and with a harder slope for the illuminating spectrum $\Gamma = 1.6$ (which increases the number of photons at high energies). To enhance the strength of the Fe K emission profile, we set the iron abundance to five times its solar value ($A_{\rm Fe}$), which is also in line with the values required to fit reflection in many accreting black holes (García et al. 2018).

Three main calculations were done, only varying the high-energy cutoff of the illuminating power law, which was set at $E_{\rm cut} = 10$, 10^2, and 10^3 keV. All other parameters were kept at the values quoted above. The main results of the full `xillver` calculations are presented in Figure 7, which includes both the reflected spectra at the surface, and the full temperature profile in the vertical direction of the atmosphere. As before, we show the comparisons of the same calculation carried out with the Gaussian and the exact redistribution functions for Compton scattering.

The largest and most obvious differences in the reflected spectrum are seen at high energies (above ∼20 keV), where the Compton kernel acts most strongly. However, for the lowest value of the high-energy cutoff ($E_{\rm cut} = 10$ keV) the results look almost identical, with very minor differences in the temperature profile at the largest optical depth. This is likely due to the lack of high-energy photons in the illumination, and the fact that the temperature never reaches extreme values. The strongest atomic features in these models are due to O (∼0.8 keV) and Fe (∼6.7 keV) K-shell emission.

We note that the peak of the emission line does not change among calculations with different redistribution functions. This is because those line-core photons are mostly emitted close to the surface, thus they suffer little to no scatterings on their way to the observer. The temperature profiles show relatively small variations between the two approximations. Only in the hottest case ($E_{\rm cut} = 1$ MeV) do we see a noticeable difference in the deepest regions of the slab, likely because the radiation field has been modified sufficiently such that the temperature solution is affected.

Evidently, the largest differences in the spectra are observed in the region of the Compton hump, and they are most marked for the models with the highest cutoff energy. This is expected, as these are the models with enough photons in the energy range where Comptonization produces the strongest redistribution, but also because the higher the $E_{\rm cut}$ the higher the overall temperature of the atmosphere.

In fact, the model with $E_{\rm cut} = 1$ MeV shows strong departures from the Gaussian approximation at all energies, even below 1 keV. One reason for the changes at soft energies is the different solution of the ionization balance, as clearly evidenced by the discrepant temperature profiles at large depths. However, a more important effect is introduced by the Comptonization solution, given that the gas temperature is close to 10^9 K in a large portion of the slab at the upper layers ($\tau_{\rm T} \sim 10^{-4} - 1$). As discussed in previous sections, in this high-temperature regime the redistribution function based on the Gaussian approximation fails most dramatically when compared to the exact solution (e.g., Figure 2). When the temperature of the atmosphere reaches such high values, the Gaussian solution of the Comptonization produces inaccurate results at all photon energies.

4. Discussion and Conclusions

In this paper we have presented a detailed discussion of the thermal Comptonization process in optically thick media. We have focused our results on the context of the reprocessed high-energy radiation in accretion disks around compact objects. Still, the approximations presented here are useful for any other problems in which accurate calculations of the Comptonized spectrum are required.

Given the intrinsic complexity of the X-ray reflection calculations, traditional models have made use of a simplified Gaussian approximation to describe the redistribution of photons in the X-ray band after suffering many scatterings in an optically thick slab. We have shown new calculations that allow adoption of a much more accurate solution for the Comptonization, taking into account the most relevant physics (i.e., quantum electrodynamical and relativistic corrections to the classical Thomson cross section). Therefore, the NP93 solution, which is the solution implemented in the present work, can be considered as *exact* within the precision of the numerical integration of the Maxwellian distribution.

Comparisons between the previously used Gaussian approximation and the exact NP93 solution reveal that the major discrepancies occur at either very high energies (typically above ∼100 keV), where electron scattering becomes most important; and/or when the gas temperature approaches $\sim 10^9$ K (regardless of the photon energy), a regime in which the thermal motions of the electrons become relativistic, causing a decrease of the Klein–Nishina cross section at energies above ∼1 keV (Figure 1). We emphasize that such high temperatures do not represent the most common conditions of accreting sources, in which coronal temperatures of hundreds of keV are typically observed (e.g., Fabian et al. 2015, 2017).

Meanwhile, the changes of the spectral shape in the Compton hump band (∼20–40 keV) observed in the reflection spectrum can potentially affect the coronal temperature derived from spectral fits. Coronal temperatures are typically estimated by measuring the cutoff at high energies of the continuum and reflection spectra (e.g., García et al. 2015; Kara et al. 2017; Buisson et al. 2019). The reflection spectra using the new Comptonization solution show a sharper cutoff than the one produced with the Gaussian solution, but depending on the parameter it might also appear at higher energies. A proper assessment of the differences in the recovered coronal temperatures from the application of these models to observational data requires the calculation of a complete grid of models covering a wide range of parameters. Such an effort is outside the scope of the present paper. However, based on the results presented in Section 3.2.3, we expect these differences to be relatively small (of the order of tens of keV or less). This is because the largest differences seem to appear when the cutoff energy (or coronal temperature) is relatively high (close to

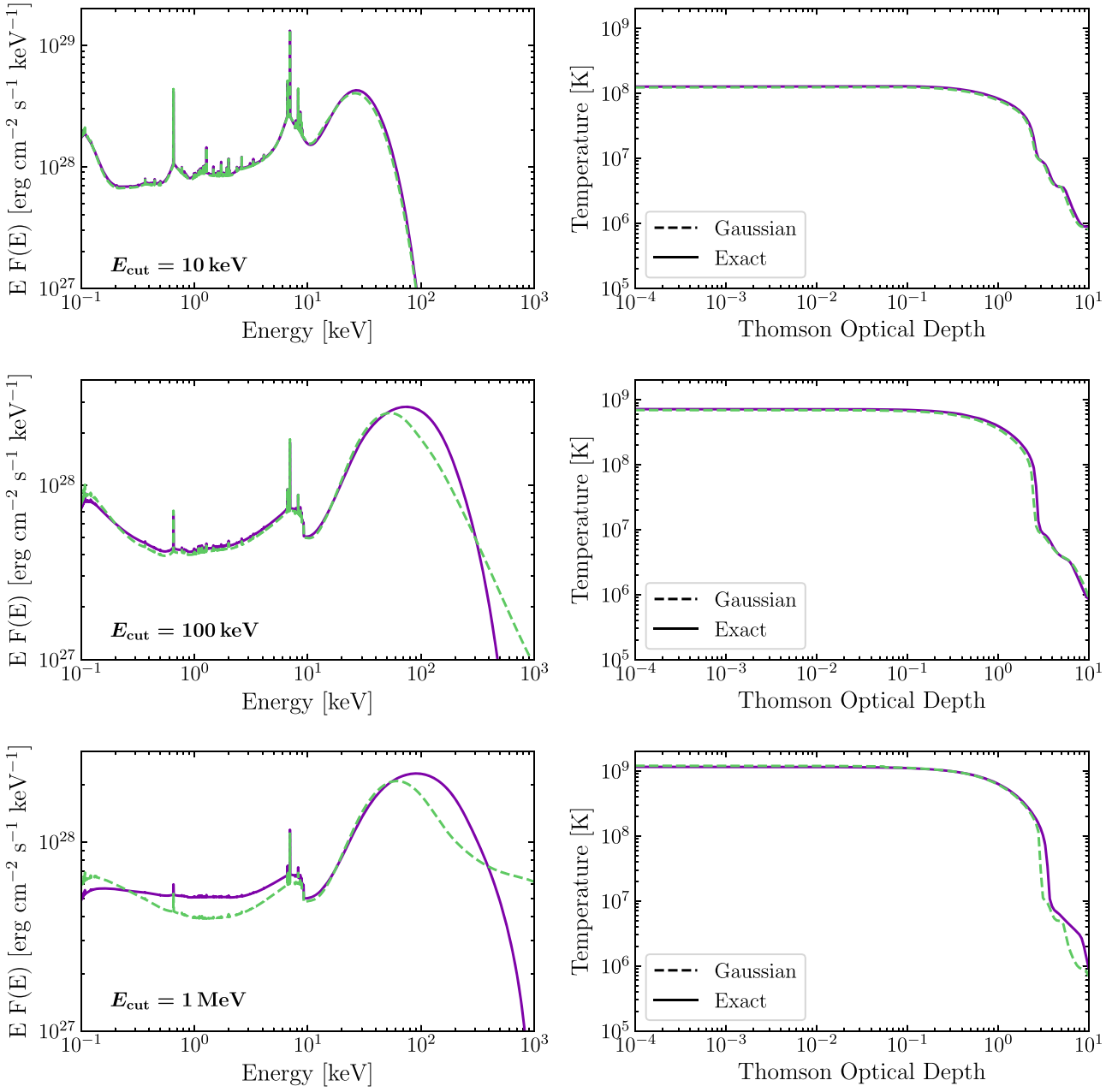

Figure 7. Full `xillver` reflection calculations for different illuminating spectra, including the solution of the ionization balance and energy equations. The left panels show the angle-averaged reflected spectrum, while the right panels show the corresponding temperature profiles in the atmosphere. The irradiation is assumed to a power law with $\Gamma = 1.4$, and 3 different high-energy cutoffs (10, 10^2, 10^3 keV), as indicated. The ionization parameter is fixed at $\xi = 3 \times 10^3$ erg cm^2 s^{-1}, and the abundance of iron is fixed at five times the solar value. Solutions using the Gaussian (dashed) and exact (solid) redistribution functions are compared.

1 MeV), while astrophysical black holes are expected (and typically observed) to have coronal temperatures of hundreds of keV or less.

Previous works on spectral models that have made use of the reflection tables produced with our `xillver` code have pointed out discrepancies found in the Compton hump at high energies, when comparing the reflected spectrum with that produced with a more accurate Monte Carlo calculation. This has motivated the use of numerical artifacts in these models, in order to try to correct for the discrepancy. Such is the case for the `xilconv` model, a modification of the `rfxconv` model (Kolehmainen et al. 2011), and first described by Done & Gierliński (2006). This model uses the `xillver` spectra below 14 keV and the Compton reflection code `pexrav` by Magdziarz & Zdziarski (1995) for higher energies. The merging of these two products requires a somewhat convoluted procedure, which is likely to reduce the self-consistency of the model. A similar approach is followed in the `reflkerr` model (Niedźwiecki et al. 2019), a more recent relativistic reflection code that also uses the `xillver` spectra for energies below ∼20 keV, and the `ireflect` model (which is a generalization of the `pexrav` model Magdziarz & Zdziarski 1995) at high energies. The new calculations presented here include the correct photon redistribution due to thermal Comptonization in the reflection calculations and will remove the necessity of modified `xillver` spectra.

The dramatic improvement brought by the new Comptonization solution to the `xillver` calculations is shown in

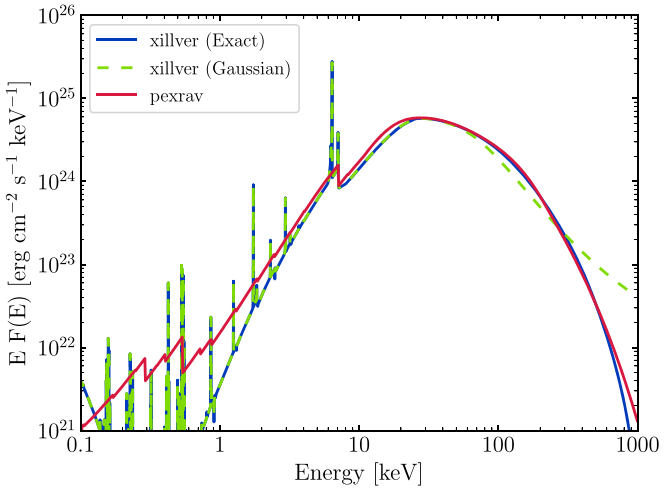

Figure 8. Comparison of the reflected angle-averaged spectra produced with `xillver` using the Gaussian approximation, the exact solution by NP93, and the calculation using the `pexrav` code, based on Monte Carlo calculations (Magdziarz & Zdziarski 1995). The parameters used are $\Gamma = 2$, $E_{\rm cut} = 300$ keV, and solar abundances for iron. The `xillver` spectra were produced for $\log(\xi/{\rm erg\ cm^2\ s^{-1}}) = 0$.

Figure 8, where we compare the angle-average-reflected spectrum generated with `xillver` using both the Gaussian and the NP93 exact solutions for Comptonization, together with the calculations using the `pexrav` model. Note that the latter is a calculation for a neutral gas (thus neglecting ionization balance), assuming electrons at rest (thus no temperature dependence in the Comptonization). Furthermore, the `pexrav` model does not include line emission, but this is unimportant for the present comparison. Nevertheless, the `pexrav` model is considered the gold-standard for Compton down-scattering. It is obvious that the `xillver` spectrum produced with the NP93 solution for Comptonization agrees very closely with that from `pexrav` at energies above ∼30 keV, where Compton scattering dominates the gas opacity. The small differences below ∼30 keV are due to the different iron photoelectric opacities implemented in the two codes. At higher energies both calculations agree very closely, except near 1 MeV, where a small divergence is seen. This is likely due to the fact that this is the upper limit of our calculations, which could affect our convolution. Moreover, the `pexrav` model is constructed using fits to detailed Monte Carlo calculations, and thus it could be prone to small numerical errors.

Importantly, the inclusion of an accurate description of the Comptonization in the reflection calculations has allowed us to verify and validate the results from spectral fits that made use of our reflection models. Based on the results presented here, we are now confident that the limitations of the Gaussian approximation used in standard modeling only manifest in extreme cases of very high temperatures, which will likely have a minor impact on the overall breadth of spectral fits of accreting compact objects published to date. Nevertheless, future releases of our `xillver` tables of reflection spectra will be computed implementing the *exact* NP93 solution described here, in an attempt to provide a more accurate prediction of the reprocessed X-ray spectrum in accretion disks. The implementation of these new models will be identical to the current version, with no additional parameters. The present versions of the codes used in this paper for the calculation of the redistribution Compton kernel are made publicly available on GitHub.[9]

This work was been partially supported under NASA No. NNG08FD60C. J.A.G. acknowledges support from NASA ATP grant No. 80NSSC20K0540 and from the Alexander von Humboldt Foundation. E.K.S and J.W. have been supported by DFG grant WI 1860/11-1. A.R., J.M., and A.M. were supported by grants No. 2015/17/B/ST9/03422 and 2015/18/M/ST9/00541 from the Polish National Science Center.

software XILLVER (García & Kallman 2010; García et al. 2013), MATPLOTLIB (version 3.1.3, Hunter 2007), NUMPY (version 1.18.1, Oliphant 2006).

ORCID iDs

Javier A. García https://orcid.org/0000-0003-3828-2448
Thomas Dauser https://orcid.org/0000-0003-4583-9048
Jerzy Madej https://orcid.org/0000-0001-8417-1509
Agata Różańska https://orcid.org/0000-0002-5275-4096
Fiona A. Harrison https://orcid.org/0000-0003-2992-8024
Jörn Wilms https://orcid.org/0000-0003-2065-5410

References

Abramowitz, M., Stegun, I. A., & Romer, R. H. 1988, AmJPh, 56, 958
Aharonian, F. A., & Atoyan, A. M. 1981, Ap&SS, 79, 321
Ballantyne, D. R. 2004, MNRAS, 351, 57
Ballantyne, D. R., Purvis, J. D., Strausbaugh, R. G., & Hickox, R. C. 2012, ApJL, 747, L35
Ballantyne, D. R., Ross, R. R., & Fabian, A. C. 2001, MNRAS, 327, 10
Ballantyne, D. R., Ross, R. R., & Fabian, A. C. 2002, MNRAS, 336, 867
Ballantyne, D. R., Turner, N. J., & Blaes, O. M. 2004, ApJ, 603, 436
Ballantyne, D. R., Turner, N. J., & Young, A. J. 2005, ApJ, 619, 1028
Brenneman, L. 2013, Measuring the Angular Momentum of Supermassive Black Holes (New York: Springer)
Buisson, D. J. K., Fabian, A. C., Barret, D., et al. 2019, MNRAS, 490, 1350
Chandrasekhar, S. 1960, Radiative Transfer (New York: Dover)
Dirac, P. A. M. 1925, MNRAS, 85, 825
Done, C., & Gierliński, M. 2006, MNRAS, 367, 659
Fabian, A. C., Lohfink, A., Belmont, R., Malzac, J., & Coppi, P. 2017, MNRAS, 467, 2566
Fabian, A. C., Lohfink, A., Kara, E., et al. 2015, MNRAS, 451, 4375
Fabian, A. C., Rees, M. J., Stella, L., & White, N. E. 1989, MNRAS, 238, 729
García, J., Dauser, T., Lohfink, A., et al. 2014, ApJ, 782, 76
García, J., Dauser, T., Reynolds, C. S., et al. 2013, ApJ, 768, 146
García, J., & Kallman, T. R. 2010, ApJ, 718, 695
García, J., Kallman, T. R., & Mushotzky, R. F. 2011, ApJ, 731, 131
García, J. A., Fabian, A. C., Kallman, T. R., et al. 2016, MNRAS, 462, 751
García, J. A., Kallman, T. R., Bautista, M., et al. 2018, in ASP Conf. Ser. 515, Workshop on Astrophysical Opacities, ed. C. Mendoza, S. Turck-Chièze, & J. Colgan (San Francisco, CA: ASP), 282
García, J. A., Steiner, J. F., McClintock, J. E., et al. 2015, ApJ, 813, 84
George, I. M., & Fabian, A. C. 1991, MNRAS, 249, 352
Guilbert, P. W. 1981, MNRAS, 197, 451
Guilbert, P. W., & Rees, M. J. 1988, MNRAS, 233, 475
Haardt, F. 1993, ApJ, 413, 680
Hua, X.-M., & Titarchuk, L. 1995, ApJ, 449, 188
Hubeny, I., & Mihalas, D. 2014, Theory of Stellar Atmospheres (Princeton, NJ: Princeton Univ. Press)
Hunter, J. D. 2007, CSE, 9, 90
Jones, F. C. 1968, PhRv, 167, 1159
Kallman, T., & Bautista, M. 2001, ApJS, 133, 221
Kara, E., García, J. A., Lohfink, A., et al. 2017, MNRAS, 468, 3489
Kershaw, D. S., Prasad, M. K., & Beason, J. D. 1986, JQSRT, 36, 273
Klein, O., & Nishina, T. 1929, ZPhy, 52, 853
Kolehmainen, M., Done, C., & Díaz Trigo, M. 2011, MNRAS, 416, 311
Laor, A. 1991, ApJ, 376, 90
Lightman, A. P., Lamb, D. Q., & Rybicki, G. B. 1981, ApJ, 248, 738

[9] `driveSRF` codebase:https://github.com/jajgarcia/exact_Compton.

Lightman, A. P., & White, T. R. 1988, ApJ, 335, 57
Madej, J., & Różańska, A. 2000, A&A, 363, 1055
Madej, J., & Różańska, A. 2004, MNRAS, 347, 1266
Madej, J., Różańska, A., Majczyna, A., & Należyty, M. 2017, MNRAS, 469, 2032
Madej, J., Różańska, A., Majczyna, A., & NaleŻyty, M. 2019, MNRAS, 484, 2831
Magdziarz, P., & Zdziarski, A. A. 1995, MNRAS, 273, 837
Markoff, S., Nowak, M. A., & Wilms, J. 2005, ApJ, 635, 1203
Matt, G., Fabian, A. C., & Ross, R. R. 1993, MNRAS, 262, 179
Matt, G., Perola, G. C., & Piro, L. 1991, A&A, 247, 25
Matt, G., Perola, G. C., Piro, L., & Stella, L. 1992, A&A, 257, 63
McClintock, J. E., Narayan, R., & Steiner, J. F. 2013, SSRv, 183, 295
McClintock, J. E., & Remillard, R. A. 2006, in Compact Stellar X-ray Sources, ed. W. Lewin & M. van der Klis (Cambridge: Cambridge Univ. Press), 157
Mihalas, D. 1978, Stellar Atmospheres (2nd ed.; San Francisco, CA: Freeman)
Münch, G. 1948, ApJ, 108, 116
Nagirner, D. I., & Poutanen, J. 1994, Single Compton Scattering, Astrophysics and Space Physics Reviews, Vol. 9 (Amsterdam: Harwood Academic)
Nagirner, D. I., & Poutanen, Y. J. 1993, AstL, 19, 262
Nayakshin, S., & Kallman, T. R. 2001, ApJ, 546, 406
Nayakshin, S., Kazanas, D., & Kallman, T. R. 2000, ApJ, 537, 833
Niedźwiecki, A., Szanecki, M., & Zdziarski, A. A. 2019, MNRAS, 485, 2942
Oliphant, T. E. 2006, A Guide to NumPy, Vol. 1
Poutanen, J., Nagendra, K. N., & Svensson, R. 1996, MNRAS, 283, 892
Remillard, R. A., & McClintock, J. E. 2006, ARA&A, 44, 49
Reynolds, C. S. 2013, CQGra, 30, 244004
Reynolds, C. S. 2019, NatAs, 3, 41
Różańska, A., & Madej, J. 2008, MNRAS, 386, 1872
Różańska, A., Madej, J., Konorski, P., & Sa owski, A. 2011, A&A, 527, A47
Ross, R. R. 1978, PhD thesis, Colorado Univ.
Ross, R. R., & Fabian, A. C. 1993, MNRAS, 261, 74
Ross, R. R., & Fabian, A. C. 2005, MNRAS, 358, 211
Ross, R. R., & Fabian, A. C. 2007, MNRAS, 381, 1697
Ross, R. R., Weaver, R., & McCray, R. 1978, ApJ, 219, 292
Shakura, N. I., & Sunyaev, R. A. 1973, A&A, 24, 337
Sunyaev, R. A., & Titarchuk, L. G. 1980, A&A, 500, 167
Thomson, J. 1906, Conduction of Electricity Through Gases, Cambridge Physical Series (Cambridge: Cambridge Univ. Press)